Annals of Nuclear Medicine Vol. 16, No. 5, 317–327, 2002

Evaluation of a commercial PET tomograph-based system for the quantitative assessment of rCBF, rOEF and $rCMRO_2$ by using sequential administration of ^{15}O-labeled compounds

Miho SHIDAHARA,*,** Hiroshi WATABE,* Kyeong Min KIM,* Hisashi OKA,* Masayoshi SAGO,* Takuya HAYASHI,* Yoshinori MIYAKE,* Yoshio ISHIDA,* Kohei HAYASHIDA,* Takashi NAKAMURA** and Hidehiro IIDA*

**Department of Investigative Radiology, National Cardio-Vascular Center, Research Institute*
***Department of Quantum and Energy Engineering, Tohoku University*

The purpose of this study was to develop a reliable and practical strategy that generates quantitative CBF and OEF maps accurately from PET data sets obtained with ^{15}O-tracers.

Sequential sinogram data sets were acquired after the administration of ^{15}O-tracers, and combined single-frame images were obtained. The delay time between sampled input function and the brain was estimated from the $H_2{}^{15}O$ study with the whole brain and the arterial time-activity curves (TACs). The whole-brain TACs were obtained from the reconstructed images (image-base method) and the sinogram data (sinogram-base method). Six methods were also evaluated for the dead-time and decay correction procedures in the process of generating a single-frame image from the dynamic sinogram.

The estimated delay values were similar with both the sinogram-based and image-based methods. A lumped correction factor to a previously added single-frame sinogram caused an underestimation of CBF, OEF and $CMRO_2$ by 16% at maximum, as compared with the correction procedure for a short sinogram. This suggested the need for a dynamic acquisition of a sinogram with a short interval. The proposed strategy provided an accurate quantification of CBF and OEF by PET with ^{15}O-tracers.

Key words: O-15 water, O-15 oxygen, positron emission tomography, arterial input function

INTRODUCTION

CEREBRAL BLOOD FLOW (CBF), Cerebral Metabolic Rate of Oxygen ($CMRO_2$), Oxygen Extraction Fraction (OEF) and Cerebral Blood Volume (CBV) can be measured by means of positron emission tomography (PET) and the administration of three ^{15}O labeled compounds, i.e. $C^{15}O$, $H_2{}^{15}O$ and $^{15}O_2$.[1] Among the approaches to estimating CBF, $CMRO_2$, OEF and CBV, the steady-state method[2–6] has been widely employed in a number of clinical studies, in which functional images were estimated from equilibrium PET images obtained during a continuous administration of each tracer. Although the steady state method is advantageous owing to its simple mathematical formulation, previous investigators reported a number of limitations. First, the steady-state method requires a physiological steady state condition for a relatively long period, namely the entire study period. This is somewhat difficult to achieve in typical clinical studies. Second, one crucial limitation of the method is the importance of its sensitivity to several error sources such as statistical noise and tissue heterogeneity.[3,5] Third, the relatively large radiation dose is considered to be an additional limitation of this approach.[7]

An alternative method is autoradiography, which is based on a single PET imaging after the non-steady state administration of a radiotracer, and can be applied to both

Received February 28, 2002, revision accepted May 9, 2002.

For reprint contact: Hidehiro Iida, Ph.D, D.Sc., Department of Investigative Radiology, National Cardio-Vascular Center Research Institute, 5–7–1 Fujishiro-dai, Suita, Osaka 565–8565, JAPAN.

E-mail: iida@ri.ncvc.go.jp

$H_2{}^{15}O$ and $^{15}O_2$ studies. The $H_2{}^{15}O$ autoradiography provides a CBF map through a PET counts-vs-CBF nomogram according to a simple table-look-up procedure.[8–10] Similarly, OEF can be estimated from an $^{15}O_2$ image in addition to additionally estimated CBF and CBV images.[11] Ohta et al.[12] proposed a similar method for the quantitation of $CMRO_2$ from the dynamic $^{15}O_2$ PET data alone, in which $CMRO_2$ was fitted to the dynamic data, to avoid the need for a separate determination of CBF and CBV.

A major advantage of these autoradiographic approaches is associated with the considerably shorter scan time than with the steady-state method,[10,11] but there are several critical processes in the autoradiographic method. Of these, a major factor is associated with the need for an accurate determination of the arterial input function. While the arterial radioactivity concentration under steady state conditions can be determined easily by drawing arterial blood stream samples with a syringe, the autoradiographic approach requires continuous monitoring of the time course of the arterial radioactivity concentration during the scan period, which is a labor-intensive task. The delay and the dispersion attributed to the prolonged transit time in the peripheral arterial lines should be taken into account.[10,13] Previous studies demonstrated that even small errors in the delay and dispersion corrections could cause serious errors in the estimated parameters, particularly when the scan duration is shortened.[14,15] The delay can be determined by using the whole-brain time-activity curve as proposed originally by Kanno et al.[10] The method has been further improved by Iida et al.,[13] but the validity of this procedure remains unknown, and practical procedures have yet to be systematically optimized. Furthermore, the $^{15}O_2$ study requires the simultaneous determination of two independent input functions, i.e., for $^{15}O_2$ itself and for metabolized $H_2{}^{15}O$.[16] The two input functions can be determined with frequent plasma separations during the arterial blood sampling, which is a major intensive process,[16] and a simplified procedure is most desirable.

Regarding image acquisition, the statistics or quality of the reconstructed image is a major concern due to the shorter scan time than with the steady state method. Although prolongation of the scan allowed the count statistics to be improved in the original PET image, the non-linear relationship between the PET counts and the parameter of interest resulted in a deterioration of the noise in the parametric images. A previous study showed that the optimal scan time that maximized the quality of the $H_2{}^{15}O$-derived CBF images was around 90 sec, for a PET study performed with a bolus i.v. injection of $H_2{}^{15}O$.[17–19] Increasing the dose of $H_2{}^{15}O$ administered improves the total counts recorded for image reconstruction, but at the expense of further accumulation of random counts, which may increase statistical noise in the net sinogram so that there should be an optimal administration dose, to maximize the image quality.

An additional factor is related to the appropriate correction procedures for dead-time and radioactivity decay, which become essential when the radioactivity distribution varies over time during the scan after the bolus administration of the ^{15}O-labeled tracers. A previous study suggested the need for real-time correction of the dead-time and the decay when acquiring the sinogram, by employing specially designed hardware.[20] On the other hand, commercially available PET scanners cannot do this, so that the sinograms need to be acquired with a short acquisition time in order to achieve accurate corrections for dead-time and radioactivity decay in the $H_2{}^{15}O$ and the $^{15}O_2$ studies.[21]

In the present study, we used a method to quantitatively assess parametric images of CBF, OEF, $CMRO_2$ and CBV from non-equilibrium PET images obtained after the injection of a series of ^{15}O-labeled compounds. The whole brain TAC was estimated from the sequential sinogram data, after applying corrections for both dead-time and radioactivity decay, which required less data space and computing time than reconstructing all the frame data sets. The dynamic sinogram was normalized for the inhomogeneous detector sensitivity, including correction for detector dead-time count losses. The scan protocol was tested on healthy volunteers, and the applicability of this protocol to clinical studies has been tested.

MATERIALS AND METHODS

Theory of parametric mapping

The cerebral blood volume, CBV is calculated from an equilibrium image obtained after a short-time inhalation of $C^{15}O$. The formula given by Mintun[11] is:

$$CBV = \frac{[PET]}{RHct \cdot \rho_{brain} \cdot A_{CO} \cdot \rho_{blood}} \qquad (1)$$

where PET is the counts per pixel of the PET image [Bq/m*l*], ρ_{brain} is the density of brain tissue (1.04) [g/m*l*], ρ_{blood} is the density of blood (1.06) [g/m*l*], RHct is the correction factor for the hematocrit difference between the peripheral and central arteries (fixed at 0.85 in this study), and A_{CO} [Bq/g] is the mean of the radiotracer concentration in the arterial blood, corrected to compensate for decay to the time of starting PET.

The cerebral blood flow, CBF, was calculated according to the method of $H_2{}^{15}O$ autoradiography.[8–10] Assuming a single tissue-compartment model, the observed tissue radioactivity concentration obtained after administration of ^{15}O-H_2O with a scan starting at time T_1 and ending at time T_2 is written as:

$$\int_{T_1}^{T_2} Ci(t)dt = \rho_{brain} \cdot \int_{T_1}^{T_2} f \cdot A(t) \otimes \exp\left[-\frac{f}{p}t\right]dt \qquad (2a)$$

where $Ci(t)$ [Bq/m*l*] is the tissue concentration of $H_2{}^{15}O$ corrected to compensate for the physical decay of ^{15}O to the scan initiation time (T_1), f [ml/min/g] is the CBF

[m*l*/min/g], $A(t)$ [Bq/m*l*] is the arterial input function, and p [m*l*/g] is the partition coefficient of water (fixed at 0.8 m*l*/m*l* in this study).[22] If the tissue and the arterial concentrations are not corrected for radioactivity decay, equation (2a) can also be given as follows:

$$\int_{T_1}^{T_2} Ci^*(t)dt = \rho_{\text{brain}} \cdot \int_{T_1}^{T_2} f \cdot A^*(t) \otimes \exp\left[-\left(\frac{f}{p}t + \lambda\right)dt\right] \quad (2b),$$

where λ is the radioactive decay constant for ^{15}O, $Ci^*(t)$ and $A^*(t)$ represent the decay-uncorrected tissue concentration and the arterial input function, respectively.

In this study, CBF was calculated by the simple autoradiographic method, in which the left member of eq. (2a) or (2b) was tabulated as a function of f with a fixed p, and the table-look-up procedure was used to generate a quantitative CBF map from the original PET image.

The oxygen extraction fraction (OEF) and the cerebral metabolic ratio of oxygen ($CMRO_2$), were calculated by the method originally proposed for the Mintun model,[11] in which the tissue radioactivity concentration observed after the inhalation of $^{15}O_2$ between time T_1 and time T_2 is given by:

$$\begin{aligned}\int_{T_1}^{T_2} Ci(t)dt &= \rho_{\text{brain}} \cdot \int_{T_1}^{T_2} \Big\{ f \cdot A_{H_2O}(t) \otimes \exp\left[-\frac{f}{p}t\right] \\ &\quad + \text{OEF} \cdot f \cdot A_{O_2}(t) \otimes \exp\left[-\frac{f}{p}t\right] \\ &\quad + \text{CBV} \cdot \text{RHct} \cdot (1 - \text{OEF} \cdot \text{Fv}) \cdot A_{O_2}(t) \Big\} dt \end{aligned} \quad (3a)$$

where $Ci(t)$ [Bq/m*l*] is the tissue radioactivity concentration at time t after inhalation of $^{15}O_2$ (physical decay was corrected back to T_1), $A_{H_2O}(t)$ [Bq/m*l*] is the arterial input function for $H_2{}^{15}O$, $A_{O_2}(t)$ [Bq/m*l*] is the arterial input function for $^{15}O_2$, VR is the small- to large-vessel hematocrit ratio (fixed at 0.85), and Fv is the effective venous fraction (fixed at 0.835). OEF images were calculated from the PET image, the input function and fixed values for p, RHct and Fv. CBF (f) were taken from the $H_2{}^{15}O$ PET study in each study. Similar to eq. (2b), the decay-uncorrected formulation of eq. (3a) can be given as:

$$\begin{aligned}\int_{T_1}^{T_2} Ci^*(t)dt &= \rho_{\text{brain}} \cdot \int_{T_1}^{T_2} \Big\{ f \cdot A^*_{H_2O}(t) \otimes \exp\left[-\left(\frac{f}{p}t + \lambda\right)\right] \\ &\quad + \text{OEF} \cdot f \cdot A_{O_2}(t) \otimes \exp\left[-\left(\frac{f}{p}t + \lambda\right)\right] \\ &\quad + \text{CBV} \cdot \text{RHct} \cdot (1 - \text{OEF} \cdot \text{Fv}) \cdot A^*_{O_2}(t) \Big\} dt \end{aligned} \quad (3b)$$

where the asterisks denote decay-uncorrected forms of the tissue concentration and the input function. $CMRO_2$ is then calculated as:

$$CMRO_2 = f \cdot \text{OEF} \cdot [O_2]_a \quad (4)$$

where f [m*l*/g/min] is the CBF obtained independently from the $H_2{}^{15}O$ study, and $[O_2]_a$ is the arterial oxygen concentration which is given as:

$$[O_2]_a = 1.39 \cdot \text{Hb} \cdot \%\text{Sat} \quad (5)$$

where 1.39 is the averaged oxygen volume associated with a single hemoglobin molecule, Hb is the hemoglobin concentration [g hemoglobin/m*l* blood] and %Sat is the percentage of saturation in O_2 of the arterial blood.

PET scan

A series of PET scans were carried out on six healthy volunteers. All subjects were male, whose age ranged from 21 to 31 (mean ± sd 24.7 ± 3.6). All subjects gave written informed consent, approved by the ethics committee of the National Cardio-Vascular Center.

The PET scanner used was an ECAT EXACT (CTI Inc. Knoxville, USA), which provided 47 tomographic slices. Sinograms were obtained dynamically in 2D mode for all scans, and the true counting rates for the whole system were recorded at every three seconds during the study.

After a 10 minute transmission scan with a rotating ^{68}Ge-^{68}Ga rod source, the first dynamic scan was started immediately after the administration of ^{15}O-CO for one minute (total administration dose was 3000 MBq (= 81 mCi)). The scan sequence was 12 × 5 sec, 4 × 15 sec, 2 × 60 sec, 1 × 240 sec, totaling 19 frames for 8 min. Approximately 10 min after the end of the ^{15}O-CO scan, gaseous ^{15}O-O_2 of 3000 MBq (81 mCi) was inhaled for 1 min, and the second dynamic scan was started at the same time as the inhalation. The scan sequence was 12 × 5 sec, 8 × 15 sec, totaling 20 frames for 3 minutes. After 10 min of radioactivity decay, another scan was started after intravenous administration of $H_2{}^{15}O$ into the right brachial vein. The dose was approximately 1110 MBq and the infusion period was 20 sec. The sequence for this scan was 12 × 5 sec, 2 × 15 sec (total 1.5 min).

Blood sampling

The concentration of radioactivity in the arterial blood was monitored continuously by means of a beta-ray detector.[10,14] A catheter was inserted into the brachial artery, and blood was withdrawn at a flow rate of 4 m*l*/min during all the PET scans. The inner diameter of the tube was approximately 1.3 mm, and the distance from the catheter to the detector was 20–25 cm. Syringe samples were also obtained during the ^{15}O-CO scan at 4, 6 and 8 min from the beginning of the scan, to measure the whole blood and plasma radioactivity concentrations. Additional samples for the $^{15}O_2$ and the $H_2{}^{15}O$ scans were obtained at 30 sec before starting the PET and 30 sec after the end of the scan, in order to measure the arterial partial pressure of CO_2 ($PaCO_2$), O_2 (PaO_2) and PH.

Cross calibration

The PET system was calibrated against the well counter system by using a cylindrical phantom with an inner diameter of 16 cm filled with ^{68}Ga solution. The count rate

per unit mass of the solution was measured with the well counter, and was referred to the pixel counts of the reconstructed PET images. This procedure was performed once, and the resulting cross calibration factor was applied to all the data sets obtained in this study. An additional calibration factor was obtained between the beta detector and the well counter for each subject. The catheter tube was filled with $H_2{}^{15}O$ saline, and its concentration was measured both with the beta detector and the well counter, to provide the sensitivity of the beta detector relative to the well counter for each catheter setup.

Data processing

Tomographic images were reconstructed by the filtered back projection method, which resulted in an observed spatial resolution of 5.8 mm full-width at half maximum (FWHM) at the center of the field of view (FOV).[23] A reconstructed image has $128 \times 128 \times 47$ slices with a pixel size of 1.84 mm × 1.84 mm and 3.38 mm. The axial resolution was approximately 5.0 mm FWHM at the center of the FOV.[23] Attenuation correction was applied with transmission data. A scatter correction was also applied by means of the deconvolution scatter function technique.[24] Correction was made also for the radioactivity decay, back to the time of the PET scan start. TAC data were collected with correction for the radioactivity decay back to the corresponding PET scan start time.

As reported in previous studies,[14,25,26] the delay and the dispersion occurring in the peripherally sampled arterial input function have been corrected carefully as follows. The dispersion time constant was first determined empirically from the dynamic $C^{15}O$ images. The arterial TACs obtained with the beta detector during the ^{15}O-CO PET scan were compared with those obtained for the regions-of-interest (ROIs) selected in the carotid artery region of the ^{15}O-CO PET images. The blood sample-based arterial TACs were deconvoluted by a previously defined dispersion function (single exponential function) with various dispersion time constants, and the optimal dispersion time constant was defined so as to best reproduce the TACs of the carotid arterial ROIs. The time-constant averaged for all the subjects was then fixed as the dispersion time-constant for the following calculation. It should be noted that the radioactivity decay of the arterial TACs was corrected prior to this dispersion correction.

The delay of the peripherally-sampled arterial TACs was determined from the $H_2{}^{15}O$ scan as described in the previous article.[13] Briefly, the arterial TAC was deconvoluted by the experimentally determined dispersion time-constant τ [sec] as described above. The whole-brain tissue radioactivity curve, $Ci(t)$ and the dispersion-corrected arterial TAC, $A(t)$ were fitted to the single-tissue compartment model, which was defined as

$$Ci(t) = K_1 \cdot A(t + \Delta t) \otimes \exp(-k_2 \cdot t) \qquad (6)$$

where Δt is the delay in the arterial TAC associated with the prolonged transit time of the peripheral artery, $A(t)$ is the dispersion- (and decay-) corrected arterial input function, K_1 and k_2 are the parameters defined in the compartment model, and $\otimes$ is the convolution operator. Three parameters Δt, K_1 and k_2 are then determined by nonlinear least squares regression analysis in each of the $H_2{}^{15}O$ scans.[13] In this work, four different protocols were employed to generate whole brain TACs, and the calculated delay values for the protocols were compared:

1. TACs were obtained by selecting an ROI that covered the whole brain in the reconstructed images.
2. TACs were obtained from dynamic sinograms including a correction for the dead-time losses.
3. TACs were obtained from dynamic sinograms excluding a correction for the dead-time losses.
4. TACs were recorded during the scan as the total prompt signals for the whole detector system, excluding the dead-time correction.

The delay value determined from the $H_2{}^{15}O$ study in each subject was also applied to the $^{15}O_2$ study, namely, the dispersion-corrected arterial (whole-blood) TAC was shifted by Δt as given from the $H_2{}^{15}O$ scan for the same subject in the same physiological condition.

To separate the metabolized $H_2{}^{15}O$ component from the $^{15}O_2$ concentration in the whole-blood radioactivity, the model-base method[16] was employed in this study, in which the metabolized $H_2{}^{15}O$ was expressed as:

$$A_{H_2O}(t) = A_{total}(t - \Delta T) \otimes \exp(-k \cdot t) \qquad (7)$$

where the parameter k is the rate constant for the production of $H_2{}^{15}O$ in the arterial blood (0.0722 min^{-1}), and ΔT is the delay in the appearance of the recirculating $H_2{}^{15}O$. The parameters k and ΔT were fixed at 0.0722 min^{-1} and 20 sec, respectively, as described in a previous work.[16] The arterial $^{15}O_2$ concentration was then estimated as

$$A_{O_2}(t) = A_{total}(t) - A_{H_2O}(t) \qquad (8)$$

Computation of functional images

The CBV image was calculated with a single frame image acquired from 4 to 8 min after inhalation of $C^{15}O$, in which the averaged radioactivity concentrations in 3 blood samples were referred to the PET images as described in eq. 1.

The dynamic PET images for the $H_2{}^{15}O$ scan were totaled for the period from 0 to 90 sec, and the autoradiographic method was applied to calculate CBF images as described above. The dynamic $^{15}O_2$ images were totaled from 0 to 3 min, and OEF images were calculated according to the autoradiographic method as described. $CMRO_2$ images were then calculated from eq. 4. A schematic diagram of the process established in this study is shown in Figure 1.

In totaling the dynamic images for $H_2{}^{15}O$ and $^{15}O_2$ scans, the following six methods for correcting the radioactivity decay and the dead-time loss in addition to the

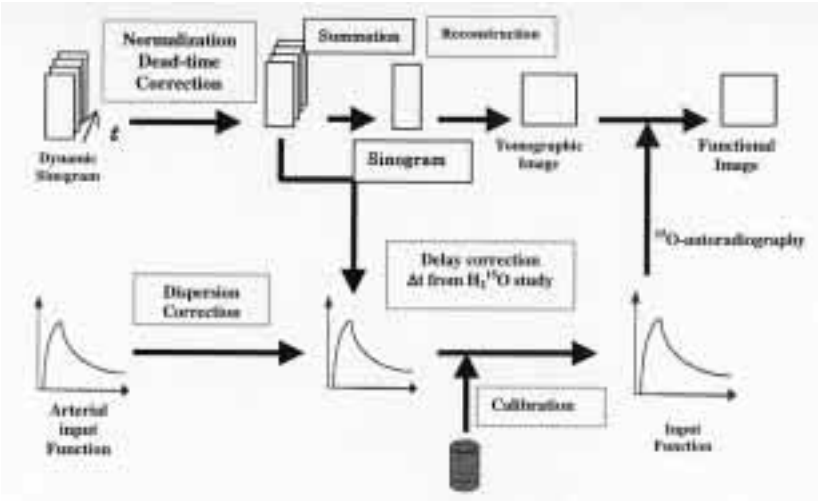

Fig. 1 Schematic diagram of the data process proposed in this study to generate quantitative CBF images. Detector normalization should be first applied to dynamic sinogram, which should then be corrected for the dead-time losses. This sinogram is used to generate the whole brain time-activity curve (TAC), which is in turn used for adjusting the delay in the peripherally sampled arterial input function. The dynamic sinogram is summed to generate a single frame image, then the autoradiographic method is applied to generate functional images.

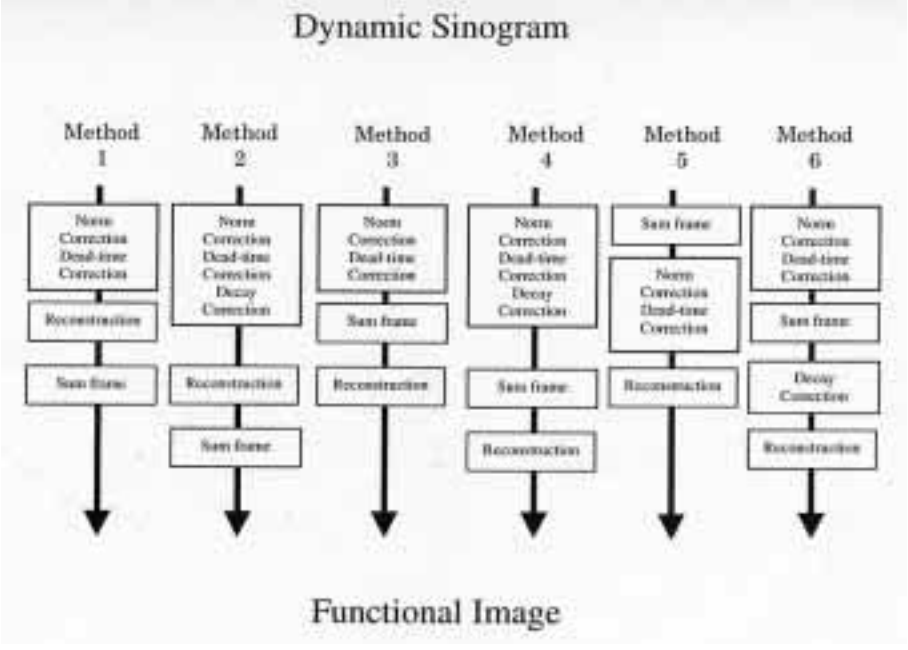

Fig. 2 Six procedures to generate a single frame summed image. Methods 1 and 2 first generated dynamic images, then the summed image was generated from the dynamic images. Methods 3 and 4 first generated summed sinogram after dead-time correction and the summed image was generated from the summed sinogram. Methods 5 first generated the summed sinogram and the summed image was generated from the summed sinogram with dead-time correction. Method 6 first generated summed sinogram without decay correction and the summed image was generated from the summed sinogram.

detector normalization were compared (see also Fig. 2). Methods 3 and 4 below were our proposed methods:

1. Dynamic sinograms were first corrected by applying detector normalization, which included dead-time correction for each frame with values determined from the system.[27] Dynamic sinograms were reconstructed, then the dynamic images were totaled for the given period. The whole brain TAC was obtained from the

dynamic images. Because physical decay correction was not applied, the functional images were calculated according to eqs. 2b and 3b.

2. Similar to the above, but the detector normalization including the dead-time correction was first applied to the dynamic sinograms and the radioactivity decay was corrected for each frame. Dynamic sinograms were reconstructed, and the dynamic images were then totaled for the given period. The whole brain TAC was also obtained from the dynamic images. Because physical decay correction was applied, the functional images were calculated according to eqs. 2a and 3a.
3. Dynamic sinograms were corrected for the dead-time losses in each frame in addition to the detector normalization. Dynamic sinograms were then summed for a given period before reconstruction. Images were reconstructed but no correction was made for radioactivity decay. The whole brain TAC was obtained from the dynamic sinogram after correction for dead-time and detector normalization. Eqs. 2b and 3b were employed to calculate functional images.
4. Dynamic sinograms were corrected for dead-time and also for the radioactivity decay in each frame, in addition to detector normalization. Dynamic sinograms were then totaled for the given period, and used for reconstruction. The whole brain TAC was obtained from the dynamic sinogram after correction for dead-time and radioactivity decay. Eqs. 2a and 3a were employed to calculate functional images.
5. Dynamic sinograms were summed for the given period without corrections for dead-time losses and radioactivity decay. The detector normalization was applied to the total sinogram. Averaged correction factors for dead-time were then applied to the totaled sinograms, but no correction was made for radioactivity decay. The totaled sinograms were then reconstructed. The whole brain TAC was obtained from the dynamic sinogram but without corrections for dead-time and normalization. Eqs. 2b and 3b were employed to calculate functional images.
6. Similar to the method 3, but with a lumped correction factor for radioactivity decay. Dynamic sinograms were corrected for the dead-time losses in addition to the detector normalization. The sinograms were totaled for the given period, and lumped correction factor for the radioactivity decay was multiplied to the totaled sinogram. These sinograms were then used for reconstruction. The whole brain TAC was obtained from the dynamic sinograms after correction for dead-time and normalization. Eqs. 2a and 3a were employed to calculate functional images.

By using the summed images with the delay- and dispersion-corrected arterial input function (the delay value was determined from the normalized sinograms in

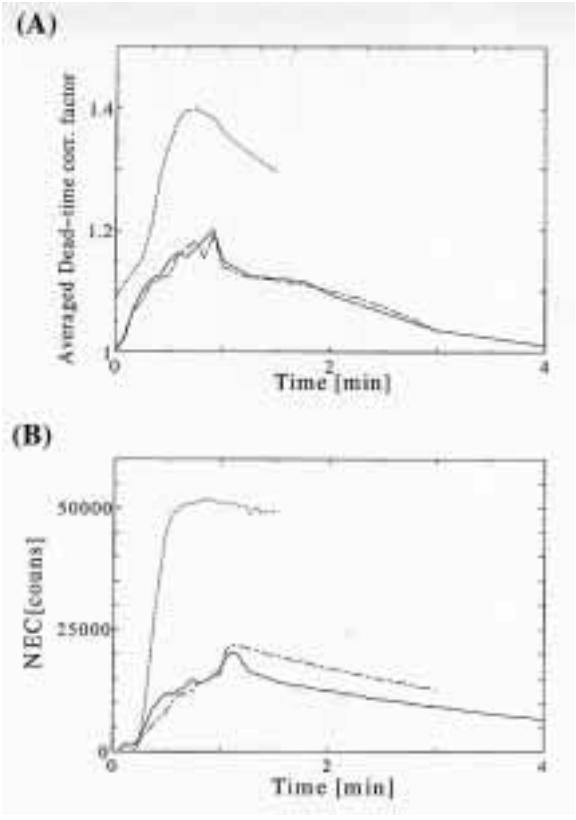

Fig. 3 Dead-time correction factors (A) and the noise-equivalent count (NEC) averaged over the slice (B), as a function of time, following each of $C^{15}O$ (*solid line*), $^{15}O_2$ (*dot-dash line*) and $H_2{}^{15}O$ (*dot line*) administration, observed in a typical study.

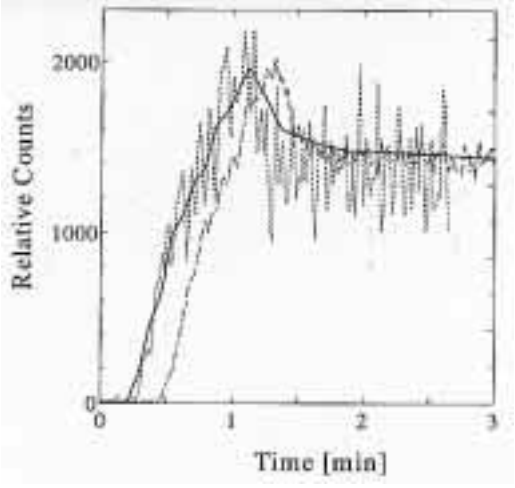

Fig. 4 Comparison of observed arterial input function, and regional time-activity curves in the area of the carotid artery, obtained following the inhalation of $C^{15}O$. The bold solid line corresponds to the regional radioactivity curve in the area of the carotid artery from the dynamic $C^{15}O$ images. The dash-dotted line corresponds to the observed beta-detector curve. The dotted line corresponds to the dispersion and delay corrected curve.

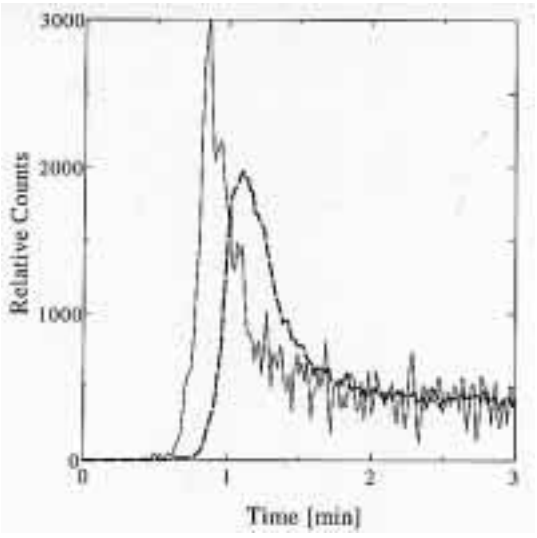

Fig. 5 A typical example of dispersion correction with the dispersion time constant of 5 sec, obtained from a typical $H_2{}^{15}O$ study. The bold dashed line corresponds to the observed beta-detector curve, and the thin solid line corresponds to the dispersion-corrected arterial input function with a dispersion time-constant of 5 sec.

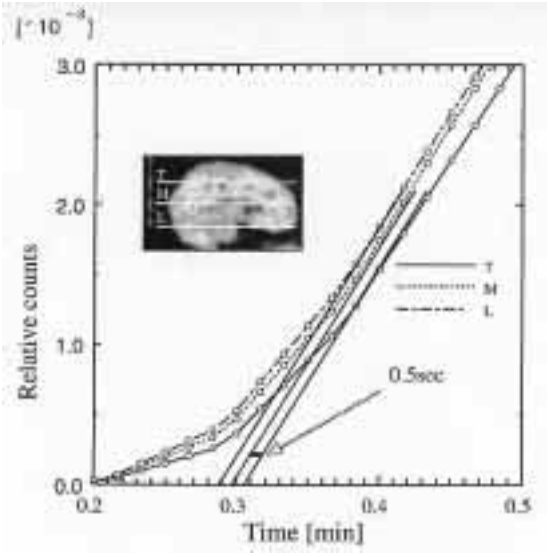

Fig. 6 Comparison of the global brain time-activity curves obtained following the administration of $H_2{}^{15}O$. The curves were compared for 4 levels of the brain regions, namely the top (T), middle (M) and the lower (L) slices, as indicated in the Figure.

Table 1 Estimated delay and k_2 values obtained from 6 normal volunteer studies with $H_2{}^{15}O$

	Reconstructed image				Sinogram with normalization				Sinogram w/o normalization				Coincidence rate from log
	Whole	Top	Middle	Low	Whole	Top	Middle	Low	Whole	Top	Middle	Low	Whole
Delay [sec]													
Mean	$9.8^{+\#}$	8.7^{*+}	$9.2^{*\#}$	$9.7^{+\#}$	$9.7^{+\#}$	8.6^{*+}	$9.2^{*\#}$	$9.7^{+\#}$	$11.0^{+*\#}$	$9.5^{\#}$	$10.4^{+\#}$	$11.2^{*+\#}$	$10.9^{*+\#}$
S.D.	1.8	1.8	1.8	1.8	1.8	1.7	1.8	1.8	1.8	1.7	1.7	1.8	1.7
k_2 [ml/g/min]													
Mean	0.757^{+}	0.719^{+}	$0.81^{*\#}$	0.774^{+}	0.766^{+}	0.74^{+}	$0.667^{*\#}$	$0.793^{+\#}$	$0.648^{*+\#}$	$0.569^{*+\#}$	0.662^{*+}	0.676^{*+}	$0.248^{*+\#}$
S.D.	0.054	0.065	0.063	0.047	0.045	0.054	0.067	0.061	0.055	0.076	0.056	0.061	0.043

*$p < 0.01$ paired t two-side test compared with image at Low slice
+$p < 0.01$ paired t two-side test compared with image at Middle slice
#$p < 0.01$ paired t two-side test compared with image at Top slice

all cases), CBF, OEF and $CMRO_2$ were calculated as described above. To compare the functional parameters among the different calculation protocols, ROIs were selected in three regions that included the whole brain, the cortical gray matter, and the white matter tissue in each subject. These ROIs were superimposed on OEF and $CMRO_2$ images and the calculated values for the protocols were compared.

All values are the mean ± one standard deviation. Student's t-test was applied to the group comparison with paired test as appropriate.

RESULTS

Figure 3 shows the dead-time correction factors and the noise-equivalent count as a function of time for the three tracer administration scans obtained from a typical study. The dead-time correction factor varies as time dependent on the counting rate after each tracer administration. The maximum correction factor was approximately 40% for the $H_2{}^{15}O$ scan, and approximately 20% for the $^{15}O_2$ and $C^{15}O$ scans.

Figure 4 shows a comparison of the observed beta-detector TAC with the ROI-based TAC in the carotid arterial region obtained from a typical $C^{15}O$ scan. The beta-detector TAC was deconvoluted by the given dispersion function with a dispersion time-constant of 5 sec to reproduce the carotid-artery TAC. The average τ value for the all studies was 4.7 ± 1.4 sec. This τ value was fixed in the following analysis. Figure 5 shows an example of the dispersion-corrected arterial input function (with $\tau = 5$ sec) obtained from a typical $H_2{}^{15}O$ scan.

Figure 6 shows TACs obtained from reconstructed PET tomographic images of top, middle and lower levels of the brain, indicating that the TAC appearance is significantly different depending on the slice level. The higher the level, the more delayed the appearance was, but the difference in transit time was approximately 0.5 sec between the lowest and the middle levels, and between the top and the middle levels. It should be noted that consistent curves are obtained also from the dynamic sinograms if the detector normalization has been applied.

The results of the delay adjustment with the 4 different protocols are summarized in Table 1. The use of the whole brain TAC obtained from the total coincidence log file resulted in a delay that was significantly longer than when determined with the reconstructed images by >1 sec in all levels (paired t-test $p < 0.01$). The sinogram yielded delay values that were in good agreement with those obtained from reconstructed images, provided that the detector normalization (including the dead-time loss) was applied in the process. The k_2 value defined in eq. 6 was 0.667–0.81 ml/min/g if the reconstructed images or the normalization-corrected sinograms are employed, whereas k_2 decreased if the total coincidence curve that were obtained from the log file or from the normalization (dead-time)-uncorrected sinogram were employed. The table also shows that the delay varies from the bottom to the top slice by approximately 1 sec, and that the whole brain TAC provided a delay value of approximately the average for the three slices. It should be further noted that the delay value between the total coincidence log and the normalization (dead-time)-uncorrected sinogram was consistent.

CBF, OEF, and $CMRO_2$ values for the whole brain, the cortical gray matter and the white matter regions are summarized in Figure 7, which compares the values for the 6 different methods. It shows that there are no significant differences between methods 1, 2, 3 and 4 except CBF for the whole brain with method 3. The average difference from method 1 is less than 2% for methods 2, 3 and 4. Method 5 (a lumped factor-based correction for the dead-time losses) resulted in computed CBF values that were underestimated compared with those obtained with methods 1–4 by a factor of 7.2% for the whole brain, 8.4% for the gray matter, and 7.4% for the white matter regions. On the other hand, OEF and $CMRO_2$ values computed by method 5 are close to the values obtained by method 1 (% difference is less than 1.5%). Method 6 (a lumped factor-based correction for radioactivity decay) gave CBF values for the whole brain that were lower by 11.7% than with method 1. Both OEF and $CMRO_2$ values obtained by method 6 were underestimated by 15.5 and 15.3%, respectively, compared with method 1.

With a UNIX workstation (Sparc Ultra 60 with 2 CPUs and 1 Gbyte Memory, Sun Microsystems Inc., CA, USA), normalization of the dynamic sinograms for an $H_2{}^{15}O$ scan (14 frames and 47 slices) required 6.3 sec. In addition, totaling of the dynamic sinogram required 1 sec. Image reconstruction for the single-frame sinogram can be completed in 15 sec, and the time for the functional image calculation of CBF was approximately 2 sec, so that the total time required for methods 3 and 4 to calculate CBF mapping was approximately 2.0 minutes. If all images were reconstructed first with method 1 or 2, the method required 5.2 minutes to complete the process. As for the O_2 study, methods 3 and 4 required 2.7 minutes for the total process, whereas methods 1 and 2 required 7.4 minutes, mostly attributed to the need for image reconstruction of a sinogram with a large number of time-frames (20 frames).

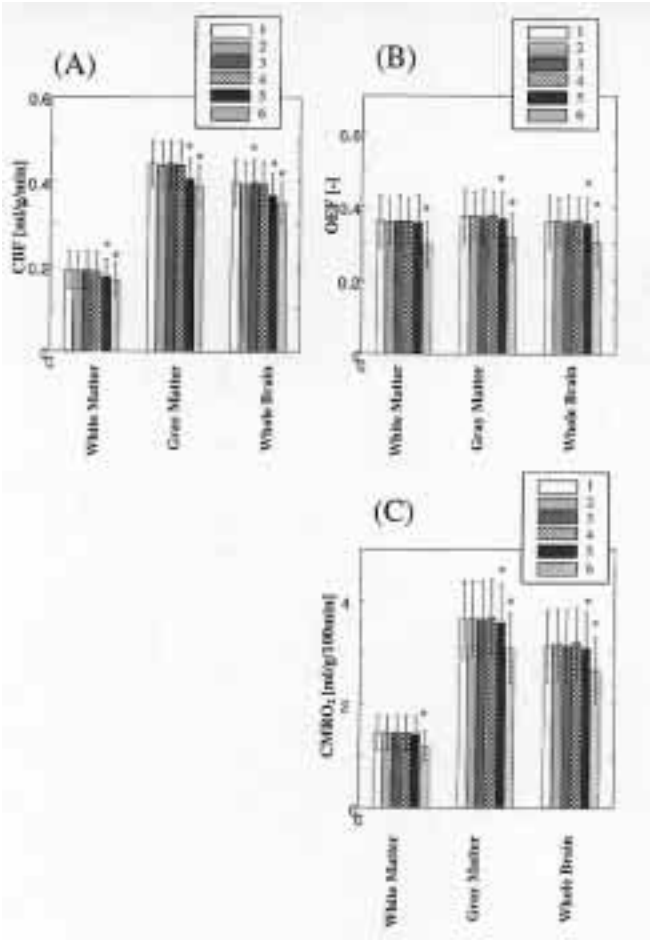

Fig. 7 A comparison of averaged (A) CBF, (B) OEF and (C) $CMRO_2$ in white matter, gray matter and whole brain between the method 1 to 6 (see in Fig. 2). A method with symbol * represents significant different from the method 1 (paired t test, $p < 0.01$)

DISCUSSION

In this study, we implemented a system to quantitatively assess CBF, OEF, $CMRO_2$ and CBV images from a series of sequential scans by using a commercial PET scanner after administration of three ^{15}O-labeled compounds. We

demonstrated that sequential acquisition of a short-period sinogram (dynamic scan) is essential in order to achieve accurate quantification of physiological parameters. This is because the dead-time count loss and physical decay vary over time, whereas the radioactivity distribution changes from region to region. To recover a radioactivity distribution that is proportional to the average of a transient distribution, the dead-time needs to be corrected frequently. Iida et al.[20] proposed a special hardware based on a real-time operation cache-memory system, which obtained a frequent dead-time correction while acquiring sinograms in the conventional histogram-mode, but this hardware has not been employed in most commercial PET scanners. In addition, whole brain TAC needs to be provided with appropriate correction for dead-time in the determination of delay in transit time in the peripherally sampled arterial input function. Kanno et al.[10] and others[13,14] proposed the use of the total coincidence counting rate obtained with PET hardware as the whole brain TAC for the determination of the global delay in transit time. This method has the advantage of not requiring dynamic acquisition, thus reducing the computation time for image reconstruction and data archiving, but the validity of this approach has not been confirmed.

In this study we showed that the delay was overestimated by more than 1 sec, if the whole brain TAC is generated without normalization or dead-time correction. This gave rise to significant systematical errors in the evaluation of the delay, which was greater than the regional variation. On the other hand, the delay time estimated from the sinogram data with dead-time correction agreed well with those from the reconstructed image, even though the attenuation correction is not applied to the sinogram data, as shown in Table 1. Kanno et al.[10] reported that 2 sec errors in delay could cause errors in CBF of approximately 5%. In addition, according to our simulation study, the 2 sec delay corresponded to errors in OEF of 4.7%. It is clear from these that the dead-time correction is essential in estimating the accurate delay from the whole brain TAC, and therefore in quantitative physiological parameters.

The dead-time correction is important in order to achieve accurate quantitation of functional images. This correction needs to be performed at each of the short period dynamic frames, as the regional distribution changes by time while the dead-time factor varies dependent on the radioactivity distribution, but was approximately a half during the $^{15}O_2$ study, and the influence of choosing a different dead-time correction method was smaller in the $^{15}O_2$ study than in the CBF study, as shown in Figure 7.

It should also be noted that the administration dose was not sub-optimal in this study, as the noise-equivalent count or NEC did not reach the maximum level, and therefore the image quality (or noise property) could be improved by increasing the dose administered. But an increased administration dose would cause more dead-time count losses, so that the dynamic acquisition of the sinogram is more crucial for generating brain TAC and reconstructing accurate distribution of radiotracers. In this study, 2D acquisition was employed, and in the future 3D will be employed in order to reduce the radiation dose. The 3D mode increases the dead-time count loss, even with a reduced administration dose. Therefore, the detector normalization that includes dead-time correction before reconstruction (method 3 or 4) becomes more important in order to reduce the calculation time, particularly in the processes of sinogram summation and reconstruction.

The comparison of methods 5 and 1 demonstrated that applying a lumped correction factor to a total sinogram resulted in systematic errors in all calculated parameters for CBF, OEF and $CMRO_2$ by −7.2, −1.5 and −1.4%, respectively. This suggests the need for sequential acquisition of short-frame sinograms in order to achieve accurate correction for dead-time. As for the decay correction, formulations are provided for the radioactivity decay being incorporated, and in fact both formulations provided results consistent with each other. Statistical noise was expected to be increased with a decay-corrected formulation, but the real clinical data did not show significantly enhanced statistical errors as compared with the decay-uncorrected formulation. This was probably attributable to the relatively short accumulation time employed in this study, namely 90 sec for the $H_2{}^{15}O$ scan, and 180 sec for the $^{15}O_2$ scan.

We propose a practical method to avoid the need for reconstructing all the dynamic frames, in which the dynamic sinogram is used only for generating the whole brain TAC with appropriate corrections for dead-time, and the image reconstruction can be applied only to the total sinogram. As shown in Figure 7, sinogram-based TAC generation (method 3 in Fig. 2) provided functional parameters which showed only a small difference as compared with the image-based TAC generation method (method 3). Only a small difference of <0.03% could be explained by numerical errors attributable to the 2-byte integer format for the image pixels. It should be noted that the total sinogram should have been corrected for the dead-time at each of the short-time frames when detector normalization is applied, as has been discussed already. Considering the time required for whole calculation and data size, this quantitative study is applicable to typical clinical studies particularly on patients with cerebral ischemic diseases.

In this study, a method for delay and dispersion correction was tested to provide an autoradiographic method. As for the OEF calculation, we employed the theory that was originally proposed by Mintun et al.,[11] which required separate scans in addition to the dynamic scan after a short-time inhalation of $^{15}O_2$. There are other methods to quantitate OEF, such as proposed by Meyer et al.[28] and by Ohta et al.[12] These methods have the advantages of providing quantitative $CMRO_2$ values without separate

scans (with the expense of increased statistical noise). Nevertheless, it should be noted that delay adjustment remains equally important in these methods, and that a dynamic acquisition with proper correction for dead-time is essential in order to determine the whole brain TAC to achieve an accurate assessment of the summed sinogram. It is obvious that the dead-time correction has to be carried out at each time frame.

Determination of delay by fitting the whole brain and arterial TACs provides two additional parameters, i.e., K_1 and k_2. Of these, K_1 is reflected in the global CBF, but it is also a function of several other factors such as the attenuation of photons in the brain, detector sensitivity, etc. Therefore, K_1 may not indicate physiologically significant values. On the other hand, k_2 does not depend on the scaling, and represents the rate of clearance of $H_2{}^{15}O$ from the brain. It is noteworthy that the estimated k_2 is consistent in the image-based and sinogram-based fitting methods.

In this study, the delay was fitted from the $H_2{}^{15}O$ scan, and the resulting value was applied to the analysis of $^{15}O_2$ data. The delay was not obtained from the $^{15}O_2$ scan because the contribution of γ rays emitted from the face mask that was supplying gaseous $^{15}O_2$ radioactivity into the subject was large, and contributed significantly to the shape of the whole brain TAC, as the spillover and the scatter from the trachea air radioactivity. We assume that the $H_2{}^{15}O$ scan should be performed under the same physiological conditions that provide the same delay value as for the $^{15}O_2$ study.

CONCLUSION

In this paper, the system has been implemented for serial PET scans with $C^{15}O$, $^{15}O_2$ and $H_2{}^{15}O$ administration. We showed the importance of dynamic data acquisition to obtain accurate physiological parameters in terms of delay estimation, dead-time correction and physical decay correction.

The computing time can be shortened by totaling frame data prior to the image reconstruction. The present system provides quantitative functional images of CBV, CBF, OEF and $CMRO_2$ with a short computing time.

REFERENCES

1. Ter-Pogossian MM, Herscovitch P. Radioactive oxygen-15 in the study of cerebral blood flow, blood volume, and oxygen metabolism. *Semin Nucl Med* 1985; 15: 377–394.
2. Subramanyam R, Alpert NM, Hoop B Jr, Brownell GL, Taveras JM. A model for regional cerebral oxygen distribution during continuous inhalation of $^{15}O_2$, $C^{15}O$ and $C^{15}O_2$. *J Nucl Med* 1978; 19: 48–53.
3. Lammertsma AA, Heather JD, Jones T, Fracowiak RSJ, Lenzi G. A statistical study of the steady state technique for measuring regional cerebral blood flow and oxygen utilization using ^{15}O. *J Comput Assist Tomogr* 1982; 6: 566–573.
4. Jones SC, Greenberg JH, Reivich M. Error analysis for the determination of cerebral blood flow with the continuous inhalation of ^{15}O-labeled carbon dioxide and positron emission tomograph. *J Comput Assist Tomogr* 1982; 6: 116–124.
5. Correia JA, Alpert NM, Buxton RB, Ackerman RH. Analysis of some errors in the measurement of oxygen extraction and oxygen consumption by the equilibrium inhalation method. *J Cereb Blood Flow Metab* 1985; 5: 591–599.
6. Okazawa H, Yamauchi H, Sugimoto K, Takahashi M, Toyoda H, Kishibe Y, et al. Quantitative Comparison of the Bolus and Steady-State Method for Measurement of Cerebral Perfusion and Oxygen Metabolism: Positron Emission Tomography Study Using ^{15}O-Gas and Water. *J Cereb Blood Flow Metab* 2001; 21: 793–803.
7. Bigler RE, Sgouros G. Biological analysis and dosimetry for ^{15}O-labeled O_2, CO_2, and CO gases administered continuously by inhalation. *J Nucl Med* 1983; 24: 431–437.
8. Raichle ME, Martin WR, Herscovitch P, Mintun MA, Markham J. Brain blood flow measured with intravenous $H_2{}^{15}O$. II. Implementation and validation. *J Nucl Med* 1983; 24: 790–798.
9. Herscovitch P, Markham J, Raichle ME. Brain blood flow measured with intravenous $H_2{}^{15}O$. I. Theory and error analysis. *J Nucl Med* 1983; 24: 782–789.
10. Kanno I, Iida H, Miura S, Murakami M, Takahashi K, Sasaki H, et al. A system for cerebral blood flow measurement using an $H_2{}^{15}O$ autoradiographic method and positron emission tomography. *J Cereb Blood Flow Metab* 1987; 7: 143–153.
11. Mintun MA, Raichle ME, Martin WR, Herscovitch P. Brain oxygen utilization measured with O-15 radiotracers and positron emission tomography. *J Nucl Med* 1984; 25: 177–187.
12. Ohta S, Meyer E, Thompson CJ, Gjedde A. Oxygen consumption of the living human brain measured after a single inhalation of positron emitting oxygen. *J Cereb Blood Flow Metab* 1992; 12: 179–192.
13. Iida H, Higano S, Tomura N, Shishido F, Kanno I, Miura S, et al. Evaluation of regional differences of tracer appearance time in cerebral tissues using [^{15}O] water and dynamic positron emission tomography. *J Cereb Blood Flow Metab* 1988; 8: 285–288.
14. Iida H, Kanno I, Miura S, Murakami M, Takahashi K, Uemura K. Error analysis of a quantitative cerebral blood flow measurement using $H_2(15)O$ autoradiography and positron emission tomography, with respect to the dispersion of the input function. *J Cereb Blood Flow Metab* 1986; 6: 536–545.
15. Dhawan V, Conti J, Mernyk M, Jarden JO, Rottenberg DA. Accuracy of PET RCBF measurements: effect of time shift between blood and brain radioactivity curves. *Phys Med Biol* 1986; 31: 507–514.
16. Iida H, Jones T, Miura S. Modeling approach to eliminate the need to separate arterial plasma in oxygen-15 inhalation positron emission tomography. *J Nucl Med* 1993; 34: 1333–1340.
17. Kanno I, Iida H, Miura S, Murakami M. Optimal scan time of oxygen-15-labeled water injection method for measurement of cerebral blood flow. *J Nucl Med* 1991; 32: 1931–1934.

18. Sadato N, Carson RE, Daube-Witherspoon ME, Campbell G, Hallett M, Herscovitch P. Optimization of noninvasive activation studies with ^{15}O-water and three-dimensional positron emission tomography. *J Cereb Blood Flow Metab* 1997; 17: 732–739.
19. Iida H, Kanno I, Miura S. Rapid measurement of cerebral blood flow with positron emission tomography Exploring the brain functional anatomy with positron tomography. In *CIBA Foundation Symposium Book 163*. John Wiley & Sons, 1991: 23–37 and discussion 37–34.
20. Iida H, Bloomfield PM, Miura S, Kanno I, Murakami M, Uemura K, et al. Effect of Real-Time Weighted Integration System for Rapid Calculation of Functional Images in Clinical Positron Emission Tomography. *IEEE Trans Med Img* 1995; 14: 116–121.
21. Van den Hoff J, Burchert W, Muller-Schauenburg W, Meyer GJ, Hundeshagen H. Accurate Local Blood Flow Measurements with Dynamic PET: Fast Determination of Input Function Delay and Dispersion by Mutilinear Minimization. *J Nucl Med* 1993; 34: 1770–1777.
22. Iida H, Kanno I, Miura S, Murakami M, Takahashi K, Uemura K. A determination of the regional brain/blood partition coefficient of water using dynamic positron emission tomography. *J Cereb Blood Flow Metab* 1989; 9: 874–885.
23. Weinhard K, Dalbom M, Eriksson L, Michel CH, Pietrzyk U, Heiss WD. Comparative performance evaluation of the ECAT EXACT and ECAT EXACT HR positron camera. In *Quantification of Brain Function. Tracer Kinetics and Image Analysis in Brain PET*, Uemura K (ed.), Amsterdam; Elsevier Science Publishers, 1993: 363–367.
24. Shao L, Karp JS. Cross-plane scattering correction-point source deconvolution in PET. *IEEE Trans Med Img* 1991; 10: 234–239.
25. Iida H, Law I, Pakkenberg B, Krarup-Hansen A, Eberl S, et al. Quantitation of regional cerebral blood flow corrected for partial volume effect using O-15 water and PET: I. Theory, error analysis, and stereologic comparison. *J Cereb Blood Flow Metab* 2000; 20: 1237–1251.
26. Law I, Iida H, Holm S, Nour S, Rostrup E, Svarer C, et al. Quantitation of regional cerebral blood flow corrected for partial volume effect using O-15 water and PET: II. Normal values and gray matter blood flow response to visual activation. *J Cereb Blood Flow Metab* 2000; 20: 1252–1263.
27. Mazoyer BM, Roos MS, Huesman RH. Dead-time correction and counting statistics for positron tomography. *Phys Med Biol* 1985; 30: 385–399.
28. Meyer E. Simultaneous correction for tracer arrival delay and dispersion in CBF measurements by the $H_2{}^{15}O$ autoradiographic method and dynamic PET. *J Nucl Med* 1989; 30: 1069–1078.